Development 135, 2173-2181 (2008) doi:10.1242/dev.017558

Ca^{2+} signals coordinate zygotic polarization and cell cycle progression in the brown alga *Fucus serratus*

John H. F. Bothwell[1], Jolanta Kisielewska[2], Martin J. Genner[1], Martin R. McAinsh[3] and Colin Brownlee[1,*]

Zygotes of the fucoid brown algae provide excellent models for addressing fundamental questions about zygotic symmetry breaking. Although the acquisition of polarity is tightly coordinated with the timing and orientation of the first asymmetric division – with zygotes having to pass through a G1/S-phase checkpoint before the polarization axis can be fixed – the mechanisms behind the interdependence of polarization and cell cycle progression remain unclear. In this study, we combine in vivo Ca^{2+} imaging, single cell monitoring of S-phase progression and multivariate analysis of high-throughput intracellular Ca^{2+} buffer loading to demonstrate that Ca^{2+} signals coordinate polarization and cell cycle progression in the *Fucus serratus* zygote. Consistent with earlier studies on this organism, and in contrast to animal models, we observe no fast Ca^{2+} wave following fertilization. Rather, we show distinct slow localized Ca^{2+} elevations associated with both fertilization and S-phase progression, and we show that both S-phase and zygotic polarization are dependent on pre-S-phase Ca^{2+} increases. Surprisingly, this Ca^{2+} requirement cannot be explained by co-dependence on a single G1/S-phase checkpoint, as S phase and zygotic polarization are differentially sensitive to pre-S-phase Ca^{2+} elevations and can be uncoupled. Furthermore, subsequent cell cycle progression through M phase is independent of localized actin polymerization and zygotic polarization. This absence of a morphogenesis checkpoint, together with the observed Ca^{2+}-dependences of S phase and polarization, show that the regulation of zygotic division in the brown algae differs from that in other eukaryotic model systems, such as yeast and *Drosophila*.

KEY WORDS: Ca^{2+}, Cell cycle, *Fucus serratus*, PCNA, Polarization, Zygote

INTRODUCTION

The coordination of cell polarization and cell cycle progression is crucial for proper zygotic development. In eukaryotes, both polarization and cell cycle progression rely on evolutionarily conserved mechanisms that include, respectively, the cytoskeletal actin nucleation machinery and cyclins/cyclin-dependent kinase (CDK) activity. These mechanisms are, in turn, coordinated by checkpoints that ensure asymmetric cell division events occur in their correct order (Hartwell and Weinert, 1989).

It follows that distinctive patterns of asymmetric division in different eukaryotic cell types may be explained largely by differences between the identity and order of checkpoints, rather than by differences between the basic mechanisms of polarization or cell cycle progression (Jensen et al., 2006; King et al., 1994). For example, in early *Drosophila* embryos, actin nucleation and DNA replication (Callaini et al., 1992; Raff and Glover, 1988) are not interdependent and this checkpoint absence promotes synchronous nuclear division (Hartwell and Weinert, 1989; Sullivan et al., 1993). Other organisms, such as *Saccharomyces cerevisiae*, show more stringent coordination of polarization and cell cycle progression, with cytoskeletal actin nucleation only beginning once cells have passed through the 'start' checkpoint of late G1/S phase (Moffat and Andrews, 2004; Singer et al., 1984). This actin nucleation is itself then monitored by a second, 'morphogenesis', checkpoint (Lew and Reed, 1995), which delays G2-to-M progression until cytoskeletal rearrangements have turned the parent cell into a characteristic 'shmoo' shape (Keaton and Lew, 2006; McMillan et al., 1998).

It is particularly important to understand such checkpoint control during eukaryotic embryogenesis, because the first asymmetric cell division defines the embryonic axes that ensure correct multicellular patterning in the adult organism (Huynh and St Johnston, 2004; Jenik and Barton, 2005). To this end, the externally fertilized gametes of brown algae provide an excellent model for developmental studies of environmentally polarized embryos (Brownlee and Bouget, 1998; Peters et al., 2008). In *Fucus serratus* zygotes, as in *S. cerevisiae*, polarization and DNA replication are both reliant on late G1/S phase CDK activity (Corellou et al., 2001b). However, the potential importance of actin and cytosolic Ca^{2+} ($[Ca^{2+}]_{cyt}$) signals – which are known to regulate CDKs in many systems (Lew and Reed, 1995; Philipova and Whitaker, 1998) – has not been addressed in this, or in any other, multicellular plant or algal zygotic model.

Specifically, although it is well established that $[Ca^{2+}]_{cyt}$ elevations follow sperm-egg fusion in a number of algal (Roberts et al., 1994), animal (Gilkey et al., 1978) and flowering plant eggs (Digonnet et al., 1997), in many of these organisms continued $[Ca^{2+}]_{cyt}$ elevations are also known to integrate subsequent developmental events (Whitaker, 2006a). In *Fucus* zygotes, localized $[Ca^{2+}]_{cyt}$ elevations are known to be essential for fertilization (Roberts et al., 1994) and polarization (Pu and Robinson, 1998; Speksnijder et al., 1989), but a potential role for post-fertilization $[Ca^{2+}]_{cyt}$ increases in initiating and co-ordinating cell cycle progression has not been explored.

In the present study, we test the hypothesis that $[Ca^{2+}]_{cyt}$ elevations coordinate actin nucleation, polarization and cell cycle progression during the first *Fucus* zygotic cell cycle. Previous attempts to study developmental $[Ca^{2+}]_{cyt}$ elevations in algal zygotes

[1]Marine Biological Association of the UK, The Laboratory, Citadel Hill, Plymouth PL1 2PB, UK. [2]University of Newcastle-upon-Tyne, Institute of Cell and Molecular Biosciences, Medical School, Framlington Place, Newcastle NE2 4HH, UK. [3]Department of Biological Sciences, Lancaster Environment Centre, Lancaster University, Lancaster LA1 4YQ, UK.

*Author for correspondence (e-mail: cbr@mba.ac.uk)

Accepted 22 April 2008

have been limited by the highly pigmented nature and scattering properties of the zygotes (Roberts et al., 1994), by difficulties in loading large numbers of eggs and zygotes with indicators or Ca^{2+} buffers, and by the absence of single cell markers for cell cycle events in vivo (Corellou et al., 2000). To overcome these problems, we use 2-photon microscopy and high-throughput biolistic loading to study how post-fertilization [Ca^{2+}] elevations direct zygotic development. Our results suggest that distinct cytosolic and nuclear [Ca^{2+}] elevations drive actin nucleation and cell cycle events, and that these [Ca^{2+}] elevations are temporally and spatially distinct from the later polarizing [Ca^{2+}] gradient. We also show that actin nucleation is essential for zygotic polarization, but not for cell cycle progression, presenting a system of asymmetric cell division control that is distinct from either the morphogenesis checkpoint-dominated yeast model or the uncoupled polarization and cell cycle model of *Drosophila* embryos.

MATERIALS AND METHODS

Plant material and culture

Mature receptacles were cut from male and female *Fucus serratus* (L.) plants and dry stored at 4°C in the dark for up to 2 weeks. Gametes were released by placing male and female receptacles in separate dishes and covering them with filtered (0.45 μm) seawater at 14°C. After 1-2 hours, released gametes were collected and eggs were either used for dye loading or mixed with sperm, with fertilization occurring within 15 minutes of gamete mixing. Eggs or zygotes were filtered through a 100 μm nylon mesh, washed twice in filtered seawater, and maintained under unidirectional light at 14°C until use.

Green fluorescent protein/proliferating cell nuclear antigen (GFP-PCNA) construct and fusion protein

The GFP fused to the human PCNA gene and containing SV40 Nuclear Localization Signal at the N terminus was a kind gift from Dr C. Cardoso (Max Delbruck Center for Molecular Medicine, Berlin, Germany). The GFP-PCNA was subcloned into the *Bam*HI/*Sac*I restriction sites of the pCal-n expression vector and its correct insertion was verified by sequencing as previously described (Kisielewska et al., 2005; Philipova et al., 2005). The GFP-PCNA protein was then expressed in BL21 competent *E. coli* cells (Promega; www.promega.com) cultured at 37°C. The protein was purified on calmodulin affinity resin (Stratagene; www.stratagene.com) according to the manufacturer's protocol.

Loading cells with metal ion buffers and fluorescent markers

All dyes and Ca^{2+} buffers were from Invitrogen (www.invitrogen.com) or Sigma (www.sigmaaldrich.com). The Ca^{2+}-sensitive fluorescent dye fura dextran (10 kDa; 4 mM), the Ca^{2+}-insensitive dyes Texas Red dextran (10 kDa; 4 mM) and fluorescein isothiocyanate dextran (FITC; 10 kDa; 20 mM), the Ca^{2+} buffers BAPTA dextran (10 kDa; 20 mM) and dibromoBAPTA (Br_2BAPTA; 40 mM), and the green fluorescent protein constructs GFP (5 mg/ml) and GFP-PCNA (3 mg/ml) were coated onto gold particles (see below) and introduced in varying combinations into *F. serratus* eggs or zygotes using a biolistic method (Bothwell et al., 2006). Control experiments using the cell-permeant heavy metal chelator N,N,N′,N′-tetrakis(2-pyridylmethyl)ethylenediamine (TPEN) were conducted by supplementing the perfusing medium with 1-100 μM TPEN or the equivalent amount of DMSO (0.2% w/v).

Parameters for the biolistic loading protocol were, briefly, as follows: 0.6 mg of 1.0 μm gold particles (Bio-Rad; www.bio-rad.com) were coated in the relevant solutions as previously described (Bothwell et al., 2006). If GFP-PCNA was being loaded, the macrocarriers were used immediately to prevent drying of the GFP-PCNA protein, otherwise macrocarriers were dried in a refrigerated drying chamber before use. Prior to biolistic loading, zygotes were transferred into filtered seawater supplemented with 0.6 M sorbitol. Around 100 μl of eggs or zygotes were then immediately transferred in a dense suspension (>100,000 cells/ml) to a 35 mm petri dish containing 3% seawater agar ~5 mm deep and subjected to biolistic bombardment using a 2200 psi rupture disc (Bothwell et al., 2006).

After loading, zygotes were settled onto 35 mm culture dishes with 0.08-0.12 mm thick coverslip bases and left in filtered seawater under unidirectional light at 14°C until needed. Loaded eggs were left to recover in filtered seawater at 14°C for 1 hour before being mixed with sperm and were treated as zygotes thereafter.

To confirm that GFP-PCNA was not denatured by biolistic loading, the localization pattern of biolistically loaded GFP-PCNA was compared with that of biolistically loaded GFP (see Fig. S1A,B in the supplementary material) or microinjected GFP-PCNA (see Fig. S1C-E in the supplementary material). For microinjection, zygotes were superfused with filtered seawater supplemented with 0.7 M sorbitol to reduce internal turgor pressure and GFP-PCNA (3 mg/ml in 200 mM KCl, 10 mM Hepes, 550 mM mannitol, pH 7.0) was pressure microinjected using dry bevelled pipettes fabricated from 1.2 mm filamented borosilicate glass (Taylor et al., 1996). No significant difference was observed between the behaviour of GFP-PCNA introduced into zygotes by microinjection or biolistic loading (see Fig. S1C-E in the supplementary material).

Fertilization assay

Cell wall secretion was monitored as a proxy for fertilization using 0.0001% Calcofluor white (CFW; Sigma) to stain cell wall cellulose. CFW fluorescence was monitored with either UV epifluorescence or 2-photon excitation (see below).

Imaging of zygotic nuclei and sperm pronuclear motion

To quantify zygotic DNA levels during early development, zygotes were stained with 100 μM Hoechst 33342 (Sigma) for 15 minutes and nuclear DNA visualized using 2-photon microscopy (see below). To measure rates of sperm pronuclear motion, sperm were stained with 100 μM Hoechst 33342 for 10 minutes and filtered through a 100 μm nylon mesh before being added to eggs. Progress of the sperm pronucleus through the egg cytoplasm was followed either with a graticule fitted to the eyepiece of an epifluorescence microscope (Swope and Kropf, 1993) or with 2-photon imaging (see below).

F-actin staining

Zygotes were fixed in buffer (2.5 mM PIPES, 1 mM $MgSO_4$, 1 mM EGTA, 0.75 M sucrose, pH 7.0 containing 0.3 mM m-maleimidobenzoyl-N-hydroxysuccinimide ester and 3.7% formaldehyde) for 30 minutes, then washed in filtered seawater and stained with 10 μM Texas Red-phalloidin for 30 minutes, before being washed twice more in filtered seawater and imaged using confocal microscopy (see below).

Confocal and 2-photon fluorescence microscopy

Dye-loaded cells were imaged with a Zeiss LSM 510 confocal/2-photon microscope (www.zeiss.com) and superfused using a gravity perfusion system. Loaded cells were imaged using a C-Apochromat 63×/1.2 n.a. water-immersion objective. All images were processed using Zeiss LSM Image Examiner software or Scion Image (www.scioncorp.com).

For confocal imaging FITC was excited using the 488 nm line of an argon/2 laser and Texas Red phalloidin excited using the 543 nm line, with emitted light bandpass filtered between 500-550 nm or 565-615 nm, respectively. Pixel images (512×512) were acquired in both cases, with four-line averaging and a pixel dwell time of 2.56 μseconds.

For all other fluorophores, the Zeiss LSM 510 was used in 2-photon mode with excitation provided by a tunable Titanium:Sapphire Mai Tai laser (Spectra Physics; www.spectraphysics.com). In all cases, 512×512 pixel images were acquired with a pixel dwell time of 2.56 μseconds and, unless stated, eight line summation. The CFW/fura dextran/Texas Red combination was excited at 780 nm with emissions monitored at 405-458 nm, 501-554 nm and 565-615 nm, respectively. Hoechst 33342 was excited at 765 nm and emitted light bandpass filtered between 435 and 485 nm. The GFP-PCNA/Texas Red marker combination was excited at 925 nm with emitted light bandpass filtered between 500-530 nm and 565-615 nm. $DiOC_6(3)$ was excited at 950 nm, with emitted light bandpass filtered between 390-465 nm and 500-550 nm and using four-line averaging.

Two-photon excitation of fura dextran at 780 nm results in decreased fluorescence with increasing [Ca^{2+}] (Wokosin et al., 2004) and [Ca^{2+}] was calculated from the R_{min} and R_{max} values of the Texas Red/fura dextran

fluorescence ratio (R) values (Grynkiewicz et al., 1985). Dye-loaded cells were superfused alternately with 50 mM Ca^{2+} seawater and Ca^{2+} free seawater (with 0.1 mM EGTA) in the presence of 100 μM ionomycin (Calbiochem; www.merckbiosciences.co.uk) to obtain R_{min} and R_{max}, respectively. Nuclear fluorescence was quantified from projections of up to 10 different confocal nuclear sections.

Quantitative determination of cell division and polarization

Ca^{2+} buffer effects on cell cycle progression and zygotic polarization were compared by measuring three parameters 24 hours after fertilization: first, cytosolic Ca^{2+} buffer concentration ($[Ca^{2+}\ buffer]_{cyt}$; biolistically loaded buffers were quantified by co-loaded FITC dextran fluorescence); second, the length/width ratio; and, third, a binary score reflecting cell cycle progression, with 0=one nucleus and no M-phase entry and 1=two nuclei and M-phase entry.

Binary scores were binomially distributed and were therefore plotted against $[Ca^{2+}\ buffer]_{cyt}$ and fitted in SYSTAT 11 (www.systat.com) to unconstrained logistic regressions of the form:

$$P = \frac{1}{\left(1 + \exp^{\beta_0 + \beta_1 x}\right)}$$

where P is the relative rate of cell cycle progression and β_1 and β_0 are constants reflecting the slope and intercept of the regression lines. The log-likelihood G^2 scores of these regressions were used to test the null hypothesis that the Ca^{2+} buffers did not affect cell cycle progression (Quinn and Keough, 2002).

Zygotic polarization in *F. serratus* is known to be S-phase dependent (Corellou et al., 2001b), so we used analysis of residuals to test a second null hypothesis: that Ca^{2+} buffers had no effects on polarization that could not be explained by their effects on S-phase inhibition. As germinated rhizoids elongate at a constant rate for at least 24 hours after S-phase entry, it follows that zygote length/width ratios are directly proportional to cell cycle progression rates. Accordingly, logistic regressions (above) were used to predict cell cycle rates in each zygote, given their $[Ca^{2+}\ buffer]_{cyt}$. Predicted length/width values were then subtracted from the measured length/width ratios to give length/width ratio residuals. Residuals were plotted against $[Ca^{2+}\ buffer]_{cyt}$ (see Fig. 5B,C) and linear regressions tested for deviations from the null model fit, i.e. the horizontal line passing through the origin.

RESULTS

GFP-PCNA can be used as a single-cell marker for DNA replication in *Fucus serratus* zygotes

To monitor post-fertilization DNA replication in individual *F. serratus* zygotes, we took advantage of the fact that, during S phase, proliferating cell nuclear antigen (PCNA) forms a highly conserved sliding clamp that is associated with active DNA polymerase (Moldovan et al., 2007). Nuclear accumulation of a GFP-PCNA chimera (Leonhardt et al., 2000) can, therefore, be used as a proxy assay for zygotic S-phase onset (Kisielewska et al., 2005).

As in sea urchin embryos (Philipova et al., 2005), *F. serratus* eggs that were co-loaded with GFP-PCNA and the marker dye Texas Red dextran showed an initial nuclear localization of GFP-PCNA (Fig. 1A), which remained constant for up to 2.5 hours after fertilization (Fig. 1B). From 3.5 hours onwards, the pattern of Texas Red dextran fluorescence remained unchanged, but the GFP-PCNA fluorescence in the nucleus began to increase relative to that in the cytosol, remaining significantly elevated ($F>5.73$, $P<0.03$) for up to 4.5 hours after fertilization (Fig. 1A,B). The timing of the nuclear GFP-PCNA elevation – around 3 hours after fertilization – matches the onset of DNA replication, as measured by nuclear staining with the DNA-binding dye Hoechst 33342 (see Fig. S2 in the supplementary material) and broadly agrees with earlier work in populations of *F. serratus* zygotes, in which increases in Histone H1 kinase activity were used as a marker for DNA replication to indicate that S-phase onset occurred around 4 hours after fertilization (Corellou et al., 2001a).

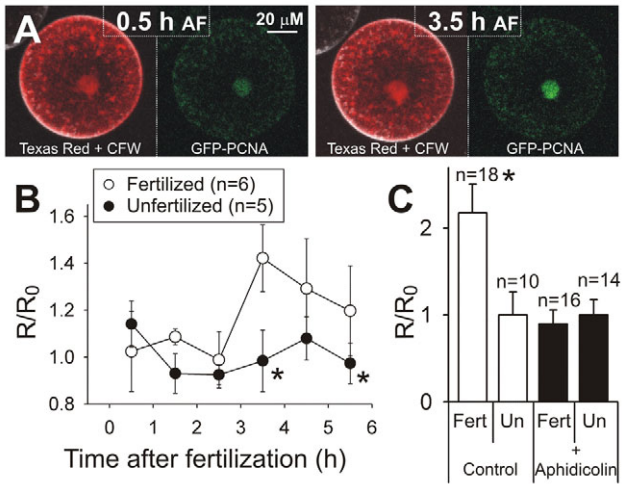

Fig. 1. GFP-PCNA is a single-cell marker of S phase in *Fucus serratus* zygotes. (**A**) Eggs were biolistically co-loaded with Texas Red dextran (red images) and GFP-PCNA (green images), and visualized using 2-photon microscopy. Fertilization was confirmed using Calcofluor white (CFW), shown as the white edge in the red images. The same representative zygote is shown 0.5 hours (left) after fertilization (AF) and 3.5 hours after fertilization (right). (**B**) Nuclear GFP-PCNA/Texas Red dextran ratios (R) were plotted relative to their starting values (R_0) for zygotes (white circles) and unfertilized eggs (black circles). Zygotes displayed significant nuclear GFP-PCNA increases between 3 and 5 hours after fertilization. Data are mean±s.e.m.; *$P<0.03$. (**C**) The nuclear GFP-PCNA increase seen 4 hours after fertilization (controls are white bars; 'Fert', zygotes; 'Un', unfertilized eggs) is completely abolished following treatment with the DNA polymerase inhibitor aphidicolin (20 μM; black bars). Data are mean±s.e.m.; *$P<0.05$.

As the present study represents the first use of GFP-PCNA in a non-animal system, we confirmed that nuclear GFP-PCNA accumulation reflected S-phase onset by noting that in sea urchin embryos the S-phase-associated nuclear accumulation of GFP-PCNA (Kisielewska et al., 2005) is reduced by the DNA polymerase inhibitor aphidicolin (Goscin and Byrnes, 1982; Ikegami et al., 1978). Accordingly, we confirmed that the post-fertilization increase in nuclear GFP-PCNA levels in *F. serratus* zygotes was completely inhibited ($F=6.86$, $P<0.001$) by aphidicolin (20 μM) applied continuously from 30 minutes after fertilization (Fig. 1C; see also Fig. S2 in the supplementary material). Taken together, these data show that GFP-PCNA can be used as a robust marker of S phase in individual *F. serratus* zygotes.

Distinct cytosolic and nuclear $[Ca^{2+}]$ elevations accompany fertilization and pronuclear fusion in *F. serratus* zygotes

To investigate whether $[Ca^{2+}]$ elevations are associated with early embryogenesis in *F. serratus*, we used 2-photon measurement of biolistically co-loaded Texas Red/fura dextran ratios to monitor cellular $[Ca^{2+}]$ during the first 3 hours of development.

The first visible sign of fertilization and egg activation was the polarized secretion of cell wall components, which progressed around the zygote at around 90±10°/minute ($n=8$; linear regression with $R^2=0.95±0.02$) and thus enclosed the zygote within 5 minutes (Fig. 2A). This was followed by a 30 minute rise in cytosolic and

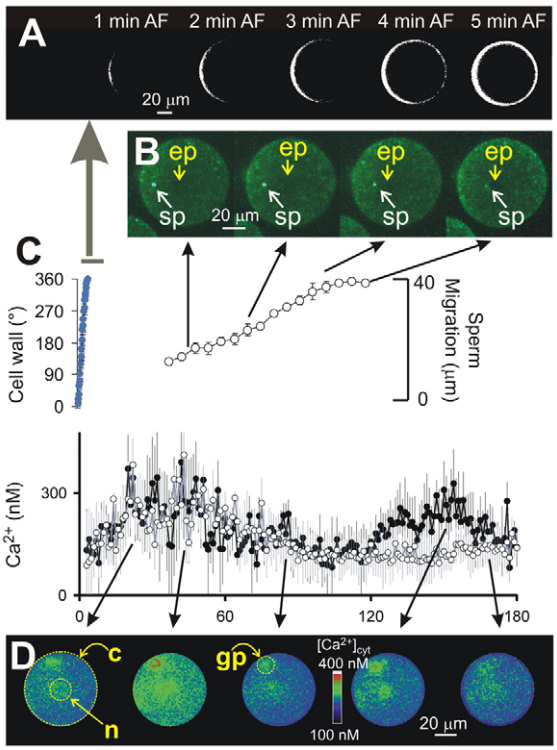

Fig. 2. Fertilization-associated events in *F. serratus*. (**A**) The first indicator of fertilization was the secretion of cell wall components, imaged using 2-photon microscopy of the cellulose stain CFW. CFW staining was evident within 15 minutes of sperm and egg mixing, and propagated across the egg within 5 minutes. (**B**) Sperm pronuclear ('sp') motion towards the egg pronucleus ('ep'), visualized using 2-photon microscopy of Hoechst 33342-labelled sperm. This representative series of images shows the sperm pronucleus as a light blue dot against a green autofluorescent background. The final image was just before pronuclear fusion. (**C**) Time courses during the first 3 hours after fertilization for cell wall secretion (upper plot, grey circles, n=8), sperm pronuclear migration (upper plot, white circles, n=10), cytosolic [Ca^{2+}] (lower plot, white circles, n=8) and nuclear [Ca^{2+}] (lower plot, black circles, n=8). Cell wall secretion is given in degrees of coverage of zygote circumference. Migration of the sperm pronucleus is given as distance into the zygote. [Ca^{2+}] was measured using Texas Red/fura dextran and divided into cytosolic and nuclear components using the regions of interest drawn in D, below. An initial sustained elevation of both cytosolic and nuclear [Ca^{2+}] was followed by a nuclear [Ca^{2+}] elevation at the time of pronuclear fusion. Data are mean±s.e.m. (**D**) Representative pseudocolour-ratiometric Texas Red/fura dextran images of post-fertilization [Ca^{2+}] changes. Regions 'c' and 'n' on the left image define, respectively, the mutually exclusive cytosolic and nuclear regions of interest. The 'gp' region is an artefact where the gold pellets (biolistic microcarriers) have gathered and can be ignored.

nuclear [Ca^{2+}], to a peak of more than 300 nM (Fig. 2C,D). We did not observe any fast cytosolic [Ca^{2+}] waves or polarized [Ca^{2+}] elevations matching the polarized pattern of cell wall secretion.

The sperm pronucleus moved towards the egg pronucleus at a steady rate of 0.31±0.02 μm/minute (n=8; linear regression with R^2=0.96±0.02) at 18-19°C (Fig. 2B,C), which compares with earlier estimates of 0.20±0.06 μm/minute at 14°C in the brown alga *Silvetia compressa* (Swope and Kropf, 1993). Given this rate of pronuclear migration, fusion of the sperm and egg pronuclei would have occurred from 2-3 hours after fertilization (Fig. 2B,C) and our results in Fig. 1 are consistent with S phase beginning after pronuclear fusion. Such post-pronuclear fusion onset of S phase has been proposed in sea urchin eggs (Longo and Plunkett, 1973), although more recent studies have shown that both PCNA (Kisielewska et al., 2005; Philipova et al., 2005) and the S phase cyclin E and cdk2 (Moreau et al., 1998; Schnackenberg and Marzluff, 2002) localize to male and female sea urchin pronuclei immediately after fertilization, suggesting that DNA replication may begin slightly before pronuclear fusion in some organisms.

After the sperm pronucleus reached the egg pronucleus, a rise in nuclear, but not in cytosolic, [Ca^{2+}] was apparent, increasing to a peak of less than 300 nM in late G1/S phase, between 2 and 3 hours after fertilization (Fig. 2C,D).

Inhibition of post-fertilization [Ca^{2+}] elevations does not affect pronuclear motion, but does suppress both actin nucleation and DNA replication

To determine whether the [Ca^{2+}] changes seen in Fig. 2 are required for zygotic polarization or cell cycle progression, we introduced the Ca^{2+} buffer, BAPTA dextran (0.4-0.8 mM), into zygotes before S-phase onset (between 30 minutes and 1 hour after fertilization), and monitored subsequent pronuclear motion, actin nucleation and nuclear GFP-PCNA localization (Fig. 3).

BAPTA dextran had no effect (F=4.54, P<0.32) on sperm pronuclear motion, with sperm pronuclei migrating towards egg pronuclei at 0.22±0.03 μm/minute in FITC dextran-loaded eggs (n=10) and 0.26±0.02 μm/minute (n=7) in BAPTA dextran-loaded eggs (Fig. 3A,B).

Untreated control zygotes showed both polarization and polarized actin nucleation (Fig. 3C), but loading zygotes with BAPTA dextran (Fig. 3D) inhibited both zygotic polarization and the cortical actin nucleation on which polarization depends (Hable and Kropf, 2000; Pu et al., 2000).

Finally, BAPTA dextran significantly inhibited (F>5.82, P<0.05) S-phase onset, as measured by nuclear GFP-PCNA accumulation (Fig. 3F).

Because previous work has shown that inhibition of CDK activity had a similar effect to our BAPTA dextran studies on zygotic polarization (Corellou et al., 2001b) and DNA replication (Corellou et al., 2001a), we treated zygotes with the cyclin-dependent kinase inhibitor olomoucine (100 μM) continuously from 20 minutes after fertilization. Olomoucine did not prevent cortical actin nucleation (Fig. 3E), although it did prevent polarization. This inability of olomoucine to mimic the full effect of BAPTA dextran suggests that separate Ca^{2+} dependencies may exist for actin nucleation and the G1/S phase checkpoint. This hypothesis is discussed further in the final Results section, below.

Cell cycle progression is not dependent on cortical actin nucleation

To investigate whether actin nucleation or localization are necessary for DNA replication and to determine whether the inhibitory effect of the Ca^{2+} buffer BAPTA dextran on DNA replication was mediated through inhibition of actin nucleation, we studied the effects of cytoskeletal actin disruption on cell cycle progression.

The actin depolymerizing agent, latrunculin B, inhibited zygotic polarization (F=45.14, P<0.001) (Fig. 4B,F) relative to controls (Fig. 4A,F) at all concentrations tested when applied continuously from 20 minutes after fertilization. Surprisingly, bearing in mind the yeast morphogenesis checkpoint, zygotes underwent complete mitosis in the presence of 0.1 μM latrunculin B, at a rate that was not significantly different (F=0.01, P<0.92) from that of untreated zygotes (Fig. 4E), to give apolar binucleate zygotes (Fig. 4B). Moreover, even

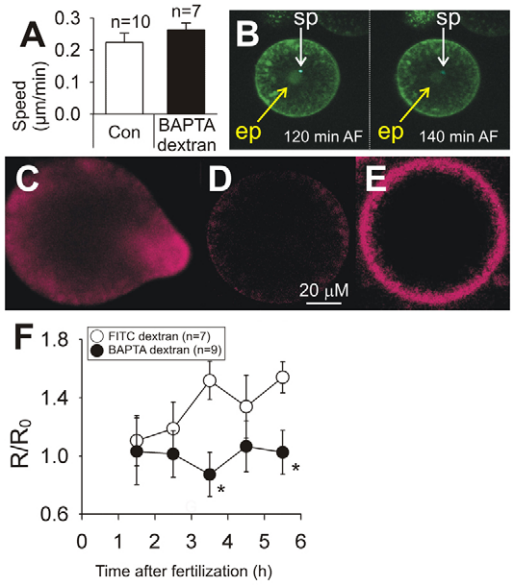

Fig. 3. Ca^{2+} buffers inhibit actin nucleation and DNA replication, but not pronuclear motion, in *F. serratus* zygotes. (**A**) The speeds at which sperm pronuclei progress towards egg pronuclei did not differ significantly between FITC-loaded and BAPTA dextran-loaded zygotes. Data are mean±s.e.m. (**B**) Pronuclear fusion in zygotes loaded with the Ca^{2+} buffer BAPTA dextran (0.4 mM). In these representative images, the sperm pronucleus ('sp') was labelled with 100 μM Hoechst 33342 and visualized using 2-photon microscopy. The left-hand image, taken 120 minutes after fertilization, shows the sperm pronucleus as a bright blue dot sitting next to the egg pronucleus ('ep') against a green FITC background (co-loaded with BAPTA dextran). In the right-hand image, taken 20 minutes later, the sperm pronucleus is less bright and has started to decondense, indicating that pronuclear fusion has started. (**C**) Untreated polarized 24-hour-old zygotes stained with Texas Red phalloidin to show actin nucleation in a cone at the germinating rhizoid apex. (**D**) Zygotes loaded biolistically with the Ca^{2+} buffer BAPTA dextran (0.4 mM) 30 minutes after fertilization and stained with Texas Red phalloidin 24 hours after fertilization. Neither zygotic polarization nor actin nucleation was observed (n=8). (**E**) Zygotes treated continuously with the CDK inhibitor olomoucine (100 μM) did not display zygotic polarization, but did show non-polarized cortical actin nucleation when stained with Texas Red phalloidin 24 hours after fertilization. (**F**) The Ca^{2+} buffer BAPTA dextran (0.4-0.8 mM) inhibited S-phase progression when loaded into zygotes 30 minutes after fertilization. Zygotes were biolistically loaded with GFP-PCNA, Texas Red dextran and BAPTA dextran and nuclear GFP-PCNA/Texas Red ratios (R) were plotted relative to their starting values (R_0) for control (white circles) and BAPTA dextran-treated zygotes (black circles). Control zygotes displayed significant nuclear GFP-PCNA increases between 3 and 5 hours after fertilization (see also Fig. 1B), but these increases were completely abolished following treatment with BAPTA dextran. Data are mean±s.e.m.; *P<0.05.

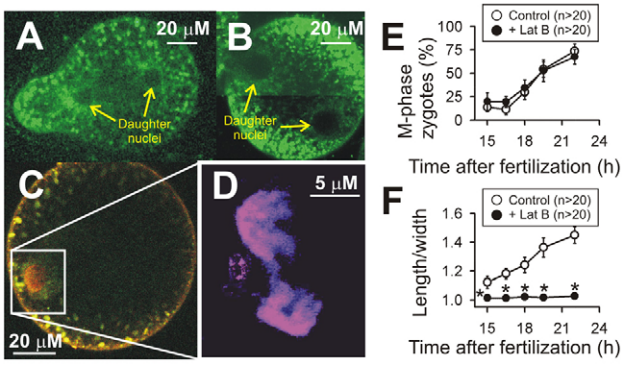

Fig. 4. Cytoskeletal actin disruption does not inhibit DNA replication. (**A**) Untreated 24-hour-old control zygotes showing zygotic polarization and mitotic division. Zygotes were loaded with 1.0 μM $DiOC_6(3)$ for 15 minutes to visualise daughter nuclei (yellow arrows) by negative staining. (**B**) Representative 24-hour-old zygote (n>100) treated with 0.1 μM latrunculin B continuously from 20 minutes after fertilization and showing complete mitosis, but no zygotic polarization or cytokinesis (no dividing cell wall). The zygote was imaged with two separate confocal scans to allow for the different depths of each daughter nucleus (yellow arrows). (**C**) Representative 24 hour old zygote (n>100) treated continuously with 1.0 μM latrunculin B. The nucleus is displaced from the usual central location, but the chromosomes are condensed, indicating M-phase entry. (**D**) Enlarged section from C highlighting condensed chromosomes. (**E**) Cytoskeletal actin disruption does not inhibit entry into M phase. Zygotes were treated with 0.1 μM latrunculin B continuously from 30 minutes after fertilization (black circles) or not treated (white circles), and scored for entry into M phase by the presence of condensed nuclei (visualized by staining with 5 μM fluorescein diacetate and 100 μM Hoechst 33342). Data are mean±s.e.m. (**F**) Cytoskeletal actin disruption does inhibit polarization. Length/width ratios were measured for the zygotes in E. Control zygotes (white circles) displayed steady growth which was completely inhibited in 0.1 μM latrunculin B-treated zygotes (black circles). Data are mean± s.e.m.; *P<0.05.

at higher latrunculin B concentrations (1.0 μM), zygotes still displayed condensed nuclei (Fig. 4C,D) that had progressed through G2/M to become arrested in M phase, although nuclei had been displaced towards the cell cortex from their normally central location (Fig. 4C).

High-throughput Ca^{2+} buffer-loading experiments confirm an S-phase Ca^{2+} requirement

Figs 2 and 3 suggest that zygotic S-phase entry in *F. serratus* requires a late G1/S-phase Ca^{2+} elevation. To provide further evidence for the importance of post-fertilization Ca^{2+} signals, zygotes were loaded either before S phase (1 hour after fertilization) or after S phase [7 hours after fertilization (Corellou et al., 2001b)] with one of four separate treatments: the high affinity (K_d ~200 nM) Ca^{2+} buffer BAPTA dextran together with FITC dextran; the moderate affinity (K_d ~1.4 μM) Ca^{2+} buffer Br_2BAPTA together with FITC dextran; FITC dextran alone; or the very low affinity (K_d ~40 μM) Ca^{2+} buffer – but very high affinity transition metal buffer – TPEN (Arslan et al., 1985).

In full support of our single-cell imaging results (Figs 2 and 3), logistic regressions fitted to these data (G^2 relative to full model=1.51, P=0.22) show that both moderate and high-affinity Ca^{2+} buffers – Br_2BAPTA and BAPTA dextran – preferentially inhibit cell cycle progression when added before S phase, with BAPTA dextran being significantly more effective than Br_2BAPTA (Fig. 5A).

Although we have used BAPTA dextran and Br_2BAPTA as Ca^{2+} buffers, they also show reasonably high affinities for other biologically important species: notably H^+ and the heavy metal ion Zn^{2+}. Although brown algal zygotes have very strong intracellular pH buffering mechanisms (Gibbon and Kropf, 1993), we nonetheless used the cell-permeant buffer TPEN (Arslan et al., 1985) as a control against any non-specific effects of BAPTA-based buffers. TPEN has much higher affinities for heavy metal ions, much lower affinity for Ca^{2+} (Kao et al., 1990) and similar pKa values (Anderegg and Wenk, 1967) to the

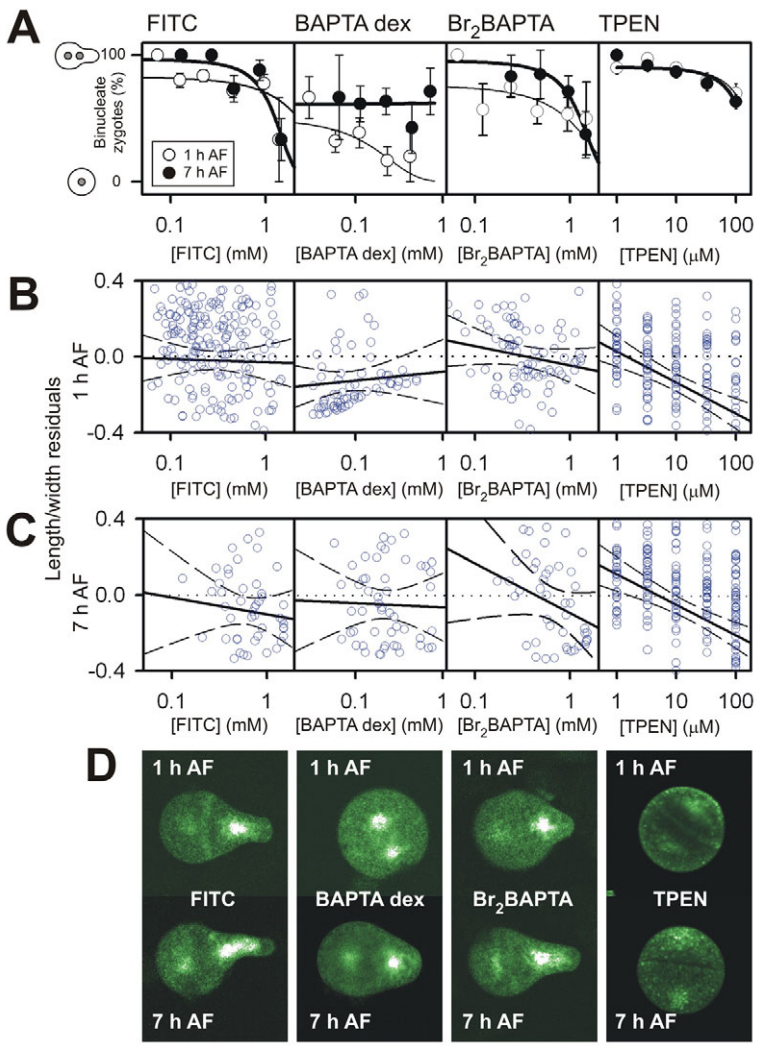

Fig. 5. Ca^{2+} buffers inhibit cell cycle progression and reveal differential effects on zygotic polarization. (**A**) The effect of Ca^{2+} buffers on cell cycle progression. Zygotes were treated 1 hour after fertilization (white circles) or 7 hours after fertilization (black circles) with one of four treatments: biolistic FITC loading, biolistic FITC+BAPTA dextran loading, biolistic FITC+Br_2BAPTA loading or superfusion with TPEN. The effect of Ca^{2+} buffers on cell cycle progression was quantified by counting the percentage of 24-hour-old zygotes that were binucleate and had clearly undergone mitosis. Buffer concentrations were lognormally distributed so the *x*-axis is logarithmic. Data are means±s.e.m. with $n>5$ for each point. (**B**) The effect of Ca^{2+} buffers on zygotic polarization when applied 1 hour after fertilization. The logistic regressions of A were used to calculate cell cycle rates for each zygote and predicted length/width ratios were subtracted from measured length/width ratios to give length/width residuals (circles). Linear regressions are shown as thick black lines, with 99% confidence limits as broken black lines. The FITC dextran and Br_2BAPTA regressions do not differ significantly from the null model (dotted horizontal line), but those for BAPTA dextran and TPEN are significantly lower than the null model. (**C**) The effect of Ca^{2+} buffers on zygotic polarization when applied 7 hours after fertilization. Data are presented as in B. The regression lines for FITC, BAPTA dextran and Br_2BAPTA do not differ significantly from the null model. However, the regression line for TPEN is significantly lower than the null model. (**D**) Representative images to show the maximum inhibition of polarization seen in binucleate zygotes. Cell cycle progression and polarization may be uncoupled either by BAPTA dextran treatment 1 hour, but not 7 hours, after fertilization or by TPEN treatment either 1 or 7 hours after fertilization.

BAPTA-based buffers (Tsien, 1980). Consistent with our hypothesis that the S-phase-specific effects of BAPTA-based buffers are mediated through Ca^{2+} binding, we did not observe preferential pre-S-phase cell cycle inhibition at TPEN concentrations with heavy metal buffering capacities equivalent to the BAPTA dextran and Br_2BAPTA concentrations used in the present study (Fig. 5A) (Kao et al., 1990).

Polarization and cell cycle progression show differential pre-S-phase Ca^{2+} requirements

Our single-cell imaging results show that Ca^{2+} buffers inhibit S-phase entry (Fig. 3F) and zygotic polarization (Fig. 3D) when introduced before S phase. Because S-phase entry and zygotic polarization in *F. serratus* are also dependent on late G1/S-phase CDK activity (Corellou et al., 2001b), it is possible that pre-S-phase Ca^{2+} elevations act solely to stimulate CDK activity (see also results for Fig. 3E, above). As no single-cell assay has been developed to measure CDK activity in individual *F. serratus* zygotes, it was not possible to test this hypothesis directly. Instead, we used multivariate analysis of residual length/width ratios (see Materials and methods) to assess the degree to which polarization and cell cycle progression relied on a common Ca^{2+}-dependent process.

The measured length-to-width ratios for FITC- or Br_2BAPTA-loaded populations do not differ significantly ($F<0.42$, $P>0.52$) from the predicted values for full dependence of polarization on cell cycle progression, regardless of the time at which buffer was loaded into zygotes (Fig. 5B,C). FITC- and Br_2BAPTA-loaded zygotes that had reached M phase had, therefore, invariably polarized (Fig. 5D). However, BAPTA dextran loaded before S phase inhibited zygotic polarization ($F=9.11$, $P<0.01$) to a degree that could not be entirely explained by the effect of BAPTA dextran on cell cycle rate alone (Fig. 5B) and that, at its most extreme, manifested itself as a complete uncoupling of nuclear division and polarization (Fig. 5D). Crucially, this additional inhibitory effect was not observed (Fig. 5C,D) when BAPTA dextran was loaded after S phase, 7 hours after fertilization ($F=0.712$, $P=0.492$), ruling out effects on post-S-phase Ca^{2+} dynamics, such as inhibition of the tip-high cytosolic [Ca^{2+}] gradient which arises just prior to rhizoid germination (Berger and Brownlee, 1993).

The heavy metal buffer TPEN was again used as a control and additionally inhibited polarization ($F>24.65$, $P<0.001$) when applied either before or after S phase (Fig. 5B-D), providing further evidence for an S-phase-specific Ca^{2+}-mediated signalling event, as inhibited by BAPTA dextran, as opposed to a general nutrient requirement for polarized growth, as inhibited by TPEN.

Taken together, the simplest explanation for our data is one in which post-fertilization Ca^{2+} elevations trigger both the G1/S-phase checkpoint and a separate, G1/S-phase checkpoint-independent,

early polarization pathway. Both processes are required for zygotic polarization, but the G1/S-phase checkpoint stimulates cell cycle progression on its own (Fig. 6A). Given our single-cell imaging results (Fig. 3), the most obvious candidate for the second, G1/S-phase checkpoint-independent, pathway is cortical actin nucleation, which is known to be required for zygotic polarization (Pu et al., 2000) and which we have shown to be Ca^{2+} dependent (Fig. 3D), but not CDK dependent (Fig. 3E). The observed uncoupling of cell cycle progression from polarization (Fig. 5B,D) also confirms the single-cell imaging results of Fig. 4 in indicating that there is no actin-based morphogenesis checkpoint for cell cycle progression in the *F. serratus* zygote.

DISCUSSION

Single cell markers are needed to study embryogenic [Ca^{2+}] signalling

Previous studies on cell cycle regulation in *F. serratus* zygotes have used whole-population assays to measure S-phase progression (Corellou et al., 2000) and CDK activity (Corellou et al., 2001b). Unfortunately, these bulk assays are not appropriate for intracellular Ca^{2+} signalling studies, because Ca^{2+} buffers and indicators may only be loaded into a small fraction of the cells present in a population (Bothwell et al., 2006). To circumvent these problems in *F. serratus* zygotes, we have adapted a GFP-PCNA single-cell assay for DNA replication (Figs 1, 3) and have used statistical analyses of polarization and cell cycle progression to test models of coupling between Ca^{2+}-dependent developmental pathways (Fig. 5).

Zygotes of *F. serratus* display a slow, global, post-fertilization [Ca^{2+}]$_{cyt}$ elevation

In all eukaryotic systems studied to date, fertilization is accompanied by intracellular [Ca^{2+}] elevations. In animal systems, these elevations generally take the form of fast [Ca^{2+}]$_{cyt}$ waves (Gilkey et al., 1978), which cross the newly fertilized egg at concentrations between 2 μM (Miyazaki, 1989) and10 μM (Brownlee and Dale, 1990; Speksnijder et al., 1990), and at speeds of around 10 μm/second (Jaffe and Creton, 1998). These fast [Ca^{2+}]$_{cyt}$ waves trigger two groups of events: zygote construction and cell cycle re-activation (Rauh et al., 2005; Whitaker, 2006a).

Evidence for such large and fast [Ca^{2+}]$_{cyt}$ waves has, however, been less forthcoming in non-animal systems, with slower [Ca^{2+}]$_{cyt}$ wave speeds of only around 1 μm/second having been recorded during in vitro fertilization in maize (Antoine et al., 2000; Digonnet et al., 1997) and with only localized cortical [Ca^{2+}]$_{cyt}$ elevations of around 300 nM having been previously reported in *F. serratus* (Roberts et al., 1994).

Here, we have used two-photon excitation for better depth penetration (Bush et al., 2007) into the highly pigmented *F. serratus* zygote to reveal the presence of a slow global post-fertilization [Ca^{2+}]$_{cyt}$ elevation (Fig. 2C,D). The polarized secretion of cell wall components that occurs within the first few minutes of fertilization may also indicate the presence of a low amplitude 'fast', post-fertilization cortical [Ca^{2+}]$_{cyt}$ wave, possibly arising from the site of sperm entry, and we cannot exclude the possibility that we have been unable to detect such a [Ca^{2+}]$_{cyt}$ elevation in *F. serratus* zygotes. However, the pattern of slow, global [Ca^{2+}]$_{cyt}$ elevation that we report here had a similar time course to the more localized [Ca^{2+}]$_{cyt}$ elevations previously reported (Roberts et al., 1994) and is consistent with the slow [Ca^{2+}]$_{cyt}$ elevations known to be associated with developmental events in a number of other organisms (Jaffe and Creton, 1998).

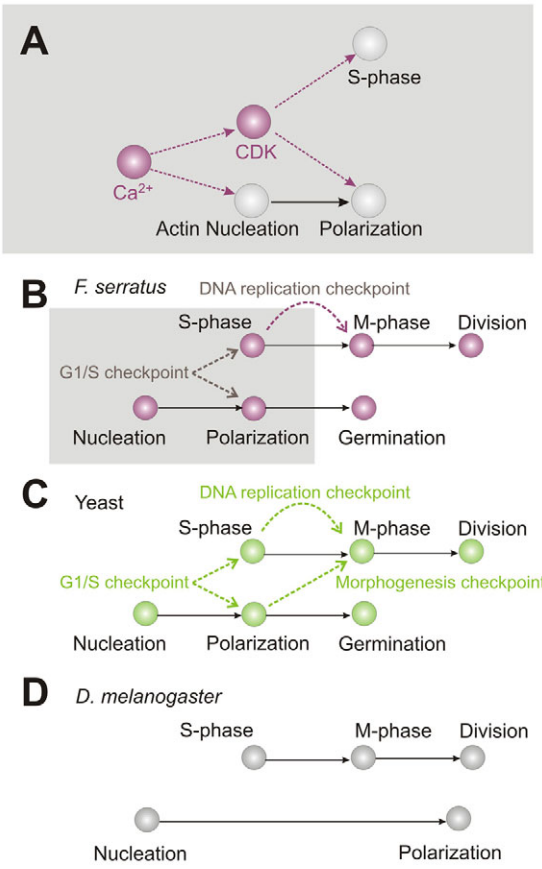

Fig. 6. Interspecific comparisons of zygotic cell cycle checkpoints. (**A**) Summary model suggested by the data in Fig. 5. Regulatory processes are represented by magenta circles and broken magenta arrows (see text for details). (**B**) The present study suggests that regulation of zygotic development in *F. serratus* is accomplished by a system of checkpoints that lie intermediate between those of the tightly coupled budding yeast (C) and the loosely coupled *Drosophila* embryo (D). Zygotic polarization and cell cycle progression in *F. serratus* are coordinated by Ca^{2+} dependent processes, but there is no dependence of the cell cycle on polarization. (**C**) In budding yeast, cell cycle progression and polarization are made interdependent by the G1/S checkpoint and the morphogenesis checkpoint. (**D**) In *Drosophila* embryos, cell cycle progression and zygotic polarization are independent, run in parallel and may be uncoupled from each other by inhibitor treatments.

Zygotic S phase is Ca^{2+} dependent in *F. serratus*

We have demonstrated that BAPTA-based buffers are able to inhibit S phase (Fig. 3F) by buffering Ca^{2+} (Fig. 5A). This Ca^{2+} dependency of zygotic S phase comes after the sperm pronucleus has migrated to the egg pronucleus (Fig. 3A,B), but before any measurable DNA replication (Fig. 3F), and strongly suggests a Ca^{2+} signalling requirement for S-phase onset.

F. serratus eggs, like sea urchin eggs and somatic cells, are arrested in G0/G1 (Corellou et al., 2001a) and must be driven into S phase following fertilization. This task is performed by the cyclin E-cdk2 complex in somatic cells (Dulic et al., 1992; Koff et al., 1992) and probably in sea urchin embryos (Schnackenberg and Marzluff, 2002). It is, therefore, interesting to note that [Ca^{2+}] elevations are able to activate both partners in the sea urchin cyclin E-cdk2 complex. For

cyclins, Ca^{2+}-dependent PKC can switch on a Na/H antiporter (Epel, 1990; Swann and Whitaker, 1985), which alkalinizes the zygote cytosol (Johnson and Epel, 1976) and leads to pH-dependent cyclin synthesis (Grainger et al., 1979; Winkler et al., 1980). For CDKs, $[Ca^{2+}]$ elevations trigger the MAP kinase ERK1 (Philipova and Whitaker, 1998), which is thought to activate cdk2 to bind the cyclin E complex (Philipova et al., 2005). Similar MAPK activation is also needed for cdk2 activity in somatic cells (Keenan et al., 2001).

Despite this potential involvement of Ca^{2+} in driving cells out of G0/G1 arrest, $[Ca^{2+}]$ elevations associated with pronuclear fusion or S-phase onset have not been well documented. There is some evidence that $[Ca^{2+}]$ elevations are associated with embryonic S-phase onset in sea urchins (Poenie et al., 1985) and $[Ca^{2+}]$ elevations are required for, but have not been visualized in, somatic S-phase (Kao et al., 1990), leading to the suggestion that they may be restricted to microdomains (Whitaker, 2006b). Our observation of a localized nuclear $[Ca^{2+}]$ elevation around the time of pronuclear fusion (Fig. 2D) offers some support for this microdomain suggestion.

Furthermore, we propose that the timing of $[Ca^{2+}]$ elevations may have a bearing on the timing of other cell cycle regulatory events. For example, sea urchin zygotes enter S-phase around 20 minutes after fertilization and an immediate post-fertilization Ca^{2+} wave may be sufficient to activate their cyclin E-cdk2 complexes, which are present in an inactive state before fertilization. *F. serratus* zygotes, however, not only have much slower rates of cell cycle progression, but also demonstrate a unique translational regulation of CDKs, which are not synthesized until several hours after fertilization (Corellou et al., 2001a). This suggests that any immediate post-fertilization $[Ca^{2+}]$ elevation could not lead to subsequent S-phase activation by Ca^{2+}-dependent MAP kinase stimulation of cdk2-cyclin, as the CDK partner would not be present. This may explain the need for a later, more prolonged $[Ca^{2+}]$ elevation of the type reported in Fig. 2D.

Pre-S-phase $[Ca^{2+}]$ elevations co-ordinate zygotic polarization and cell cycle progression

It is tempting to speculate that the post-fertilization $[Ca^{2+}]_{cyt}$ elevation that we have observed (Fig. 2C,D) acts to trigger one set of zygote activation events, such as actin nucleation (Muto and Mikoshiba, 1998), and the later nuclear Ca^{2+} elevation (Fig. 2C,D) acts to trigger another set, such as cell cycle progression. Nonetheless, although our Ca^{2+} buffer loading results suggest that the post-fertilization $[Ca^{2+}]_{cyt}$ elevation is not sufficient to drive S phase, the roles played by distinct Ca^{2+} elevations remain to be determined. Our results do, however, suggest that such distinct Ca^{2+}-dependent pathways exist (Figs 3, 5) and the simplest model for our data is one in which actin nucleation and the G1/S-phase checkpoint have independent Ca^{2+} requirements (Fig. 6A).

Absence of a morphogenesis checkpoint for cell cycle progression

In budding yeast, the joint activation of cell cycle progression and polarization by the G1/S-phase checkpoint is followed by their further coordination at the well-established morphogenesis checkpoint, in which actin localization at the bud collar is needed to bring about release of cell cycle arrest at G2/M (Keaton and Lew, 2006). However, our results clearly indicate that a morphogenesis checkpoint does not operate in the *F. serratus* zygote. The evidence for this is twofold. First, exogenous Ca^{2+} buffers are able to inhibit actin localization and zygotic polarization while allowing cell division, albeit at relatively low frequencies (Fig. 5D), which indicates that there is no absolute requirement for an actin-localization based checkpoint. Second, there is no effect on cell cycle progression to M phase when actin polymerization is inhibited sufficiently to block polarization completely (Fig. 4), which is both direct evidence against the involvement of a morphogenesis checkpoint and a surprising finding, given the demonstrated ability of actin to regulate developmental Ca^{2+} elevations in *F. serratus* zygotes (Pu et al., 2000).

The absence of a strict actin-based polarity checkpoint in the *F. serratus* zygote presents a developmental model (Fig. 6B) that is distinct from both the tightly controlled yeast morphogenesis system (Fig. 6C) and that of *Drosophila*, in which early embryonic cell cycle checkpoints are absent (Fig. 6D). This emphasises the diversity of cell cycle control in relation to polarization in different organisms.

We are grateful to the BBSRC and NERC for financial support. M. Tristan Fabre provided help with the Texas Red phalloidin staining, Dr C. Cardoso (Max Delbruck Center for Molecular Medicine, Berlin, Germany) kindly provided the GFP-PCNA construct and we thank Prof. Michael Whitaker (University of Newcastle, Newcastle-upon-Tyne, UK) for a number of helpful discussions. J.H.B. is funded by a Leverhulme Trust Early Career Fellowship and J.K. is funded by a Royal Society Dorothy Hodgkin Fellowship.

Supplementary material

Supplementary material for this article is available at http://dev.biologists.org/cgi/content/full/135/12/2173/DC1

References

Anderegg, G. and Wenk, F. (1967). Pyridinderivate als Komplexbildner VIII. Die Herstellung je eines neuen vier- and sechszähnigen Liganden. *Helv. Chim. Acta* **50**, 2330-2332.

Antoine, A. F., Faure, J. E., Cordeiro, S., Dumas, C., Rougier, M. and Feijo, J. A. (2000). A calcium influx is triggered and propagates in the zygote as a wavefront during in vitro fertilization of flowering plants. *Proc. Natl. Acad. Sci. USA* **97**, 10643-10648.

Arslan, P., Di Virgilio, F., Beltrame, M., Tsien, R. Y. and Pozzan, T. (1985). Cytosolic Ca^{2+} homeostasis in Ehrlich and Yoshida carcinomas. A new, membrane-permeant chelator of heavy metals reveals that these ascites tumor cell lines have normal cytosolic free Ca^{2+}. *J. Biol. Chem.* **260**, 2719-2727.

Berger, F. and Brownlee, C. (1993). Ratio confocal imaging of free cytoplasmic calcium gradients in polarising and polarised Fucus zygotes. *Zygote* **1**, 9-15.

Bothwell, J. H., Brownlee, C., Hetherington, A. M., Ng, C. K., Wheeler, G. L. and McAinsh, M. R. (2006). Biolistic delivery of Ca^{2+} dyes into plant and algal cells. *Plant J.* **46**, 327-335.

Brownlee, C. and Dale, B. (1990). Temporal and spatial correlation of fertilization current, calcium waves and cytoplasmic contraction in eggs of Ciona intestinalis. *Proc. R. Soc. Lond. B Biol. Sci.* **239**, 321-328.

Brownlee, C. and Bouget, F. Y. (1998). Polarity determination in Fucus: from zygote to multicellular embryo. *Semin. Cell Dev. Biol.* **9**, 179-185.

Bush, P. G., Wokosin, D. L. and Hall, A. C. (2007). Two-versus one photon excitation laser scanning microscopy: critical importance of excitation wavelength. *Front. Biosci.* **12**, 2646-2657.

Callaini, G., Dallai, R. and Riparbelli, M. G. (1992). Cytochalasin induces spindle fusion in the syncytial blastoderm of the early Drosophila embryo. *Biol. Cell* **74**, 249-254.

Corellou, F., Bisgrove, S. R., Kropf, D. L., Meijer, L., Kloareg, B. and Bouget, F. Y. (2000). A S/M DNA replication checkpoint prevents nuclear and cytoplasmic events of cell division including centrosomal axis alignment and inhibits activation of cyclin-dependent kinase-like proteins in fucoid zygotes. *Development* **127**, 1651-1660.

Corellou, F., Brownlee, C., Detivaud, L., Kloareg, B. and Bouget, F. Y. (2001a). Cell cycle in the fucus zygote parallels a somatic cell cycle but displays a unique translational regulation of cyclin-dependent kinases. *Plant Cell* **13**, 585-598.

Corellou, F., Brownlee, C., Kloareg, B. and Bouget, F. Y. (2001b). Cell cycle-dependent control of polarised development by a cyclin-dependent kinase-like protein in the Fucus zygote. *Development* **128**, 4383-4392.

Digonnet, C., Aldon, D., Leduc, N., Dumas, C. and Rougier, M. (1997). First evidence of a calcium transient in flowering plants at fertilization. *Development* **124**, 2867-2874.

Dulic, V., Lees, E. and Reed, S. I. (1992). Association of human cyclin E with a periodic G1-S phase protein kinase. *Science* **257**, 1958-1961.

Epel, D. (1990). The initiation of development at fertilization. *Cell Differ. Dev.* **29**, 1-12.

Gibbon, B. C. and Kropf, D. L. (1993). Intracellular pH and its regulation in Pelvetia zygotes. *Dev. Biol.* **157**, 259-268.

Gilkey, J. C., Jaffe, L. F., Ridgway, E. B. and Reynolds, G. T. (1978). A free calcium wave traverses the activating egg of the medaka, Oryzias latipes. *J. Cell Biol.* **76**, 448-466.
Goscin, L. P. and Byrnes, J. J. (1982). DNA polymerase delta: one polypeptide, two activities. *Biochemistry* **21**, 2513-2518.
Grainger, J. L., Winkler, M. M., Shen, S. S. and Steinhardt, R. A. (1979). Intracellular pH controls protein synthesis rate in the sea urchin egg and early embryo. *Dev. Biol.* **68**, 396-406.
Grynkiewicz, G., Poenie, M. and Tsien, R. Y. (1985). A new generation of Ca^{2+} indicators with greatly improved fluorescence properties. *J. Biol. Chem.* **260**, 3440-3450.
Hable, W. E. and Kropf, D. L. (2000). Sperm entry induces polarity in fucoid zygotes. *Development* **127**, 493-501.
Hartwell, L. H. and Weinert, T. A. (1989). Checkpoints-controls that ensure the order of cell-cycle events. *Science* **246**, 629-634.
Huynh, J. R. and St Johnston, D. (2004). The origin of asymmetry: early polarisation of the Drosophila germline cyst and oocyte. *Curr. Biol.* **14**, R438-R449.
Ikegami, S., Taguchi, T., Ohashi, M., Oguro, M., Nagano, H. and Mano, Y. (1978). Aphidicolin prevents mitotic cell division by interfering with the activity of DNA polymerase-alpha. *Nature* **275**, 458-460.
Jaffe, L. F. and Creton, R. (1998). On the conservation of calcium wave speeds. *Cell Calcium* **24**, 1-8.
Jenik, P. D. and Barton, M. K. (2005). Surge and destroy: the role of auxin in plant embryogenesis. *Development* **132**, 3577-3585.
Jensen, L. J., Jensen, T. S., de Lichtenberg, U., Brunak, S. and Bork, P. (2006). Co-evolution of transcriptional and posttranslational cell-cycle regulation. *Nature* **443**, 594-597.
Johnson, J. D. and Epel, D. (1976). Intracellular pH and activation of sea urchin eggs after fertilisation. *Nature* **262**, 661-664.
Kao, J. P., Alderton, J. M., Tsien, R. Y. and Steinhardt, R. A. (1990). Active involvement of Ca^{2+} in mitotic progression of Swiss 3T3 fibroblasts. *J. Cell Biol.* **111**, 183-196.
Keaton, M. A. and Lew, D. J. (2006). Eavesdropping on the cytoskeleton: progress and controversy in the yeast morphogenesis checkpoint. *Curr. Opin. Microbiol.* **9**, 540-546.
Keenan, S. M., Bellone, C. and Baldassare, J. J. (2001). Cyclin-dependent kinase 2 nucleocytoplasmic translocation is regulated by extracellular regulated kinase. *J. Biol. Chem.* **276**, 22404-22409.
King, R. W., Jackson, P. K. and Kirschner, M. W. (1994). Mitosis in transition. *Cell* **79**, 563-571.
Kisielewska, J., Lu, P. and Whitaker, M. (2005). GFP-PCNA as an S-phase marker in embryos during the first and subsequent cell cycles. *Biol. Cell* **97**, 221-229.
Koff, A., Giordano, A., Desai, D., Yamashita, K., Harper, J. W., Elledge, S., Nishimoto, T., Morgan, D. O., Franza, B. R. and Roberts, J. M. (1992). Formation and activation of a cyclin E-cdk2 complex during the G1 phase of the human cell cycle. *Science* **257**, 1689-1694.
Leonhardt, H., Rahn, H. P., Weinzierl, P., Sporbert, A., Cremer, T., Zink, D. and Cardoso, M. C. (2000). Dynamics of DNA replication factories in living cells. *J. Cell Biol.* **149**, 271-280.
Lew, D. J. and Reed, S. I. (1995). Cell cycle control of morphogenesis in budding yeast. *Curr. Opin. Genet. Dev.* **5**, 17-23.
Longo, F. J. and Plunkett, W. (1973). The onset of DNA synthesis and its relation to morphogenetic events of the pronuclei in activated eggs of the sea urchin, Arbacia punctulata. *Dev. Biol.* **30**, 56-67.
McMillan, J. N., Sia, R. A. and Lew, D. J. (1998). A morphogenesis checkpoint monitors the actin cytoskeleton in yeast. *J. Cell Biol.* **142**, 1487-1499.
Miyazaki, S. (1989). Calcium wave in activating hamster eggs. *Biol. Bull.* **176**, 21-24.
Moffat, J. and Andrews, B. (2004). Late-G1 cyclin-CDK activity is essential for control of cell morphogenesis in budding yeast. *Nat. Cell Biol.* **6**, 59-66.
Moldovan, G. L., Pfander, B. and Jentsch, S. (2007). PCNA-the maestro of the replication fork. *Cell* **129**, 665-679.
Moreau, J. L., Marques, F., Barakat, A., Schatt, P., Lozano, J. C., Peaucellier, G., Picard, A. and Geneviere, A. M. (1998). Cdk2 activity is dispensable for the onset of DNA replication during the first mitotic cycles of the sea urchin early embryo. *Dev. Biol.* **200**, 182-197.
Muto, A. and Mikoshiba, K. (1998). Activation of inositol 1,4,5-trisphosphate receptors induces transient changes in cell shape of fertilized Xenopus eggs. *Cell Motil. Cytoskeleton* **39**, 201-208.
Peters, A. F., Scornet, D., Ratin, M., Charrier, B., Monnier, A., Merrien, Y., Corre, E., Coelho, S. M. and Cock, J. M. (2008). Life-cycle-generation-specific developmental processes are modified in the immediate upright mutant of the brown alga Ectocarpus siliculosus. *Development* **135**, 1503-1512.
Philipova, R. and Whitaker, M. (1998). MAP kinase activity increases during mitosis in early sea urchin embryos. *J. Cell Sci.* **111**, 2497-2505.
Philipova, R., Kisielewska, J., Lu, P., Larman, M., Huang, J. Y. and Whitaker, M. (2005). ERK1 activation is required for S-phase onset and cell cycle progression after fertilization in sea urchin embryos. *Development* **132**, 579-589.
Poenie, M., Alderton, J., Tsien, R. Y. and Steinhardt, R. A. (1985). Changes of free calcium levels with stages of the cell division cycle. *Nature* **315**, 147-149.
Pu, R. and Robinson, K. R. (1998). Cytoplasmic calcium gradients and calmodulin in the early development of the fucoid alga Pelvetia compressa. *J. Cell Sci.* **111**, 3197-3207.
Pu, R. S., Wozniak, M. and Robinson, K. R. (2000). Cortical actin filaments form rapidly during photopolarization and are required for the development of calcium gradients in Pelvetia compressa zygotes. *Dev. Biol.* **222**, 440-449.
Quinn, G. P. and Keough, M. J. (2002). *Experimental Design and Data Analysis for Biologists*. Cambridge: Cambridge University Press.
Raff, J. W. and Glover, D. M. (1988). Nuclear and cytoplasmic mitotic-cycles continue in Drosophila embryos in which DNA-synthesis is inhibited with aphidicolin. *J. Cell Biol.* **107**, 2009-2019.
Rauh, N. R., Schmidt, A., Bormann, J., Nigg, E. A. and Mayer, T. U. (2005). Calcium triggers exit from meiosis II by targeting the APC/C inhibitor XErp1 for degradation. *Nature* **437**, 1048-1052.
Roberts, S. K., Gillot, I. and Brownlee, C. (1994). Cytoplasmic calcium and *Fucus* egg activation. *Development* **120**, 155-163.
Schnackenberg, B. J. and Marzluff, W. F. (2002). Novel localization and possible functions of cyclin E in early sea urchin development. *J. Cell Sci.* **115**, 113-121.
Singer, R. A., Bedard, D. P. and Johnston, G. C. (1984). Bud formation by the yeast Saccharomyces-cerevisiae is directly dependent on start. *J. Cell Biol.* **98**, 678-684.
Speksnijder, J. E., Miller, A. L., Weisenseel, M. H., Chen, T. H. and Jaffe, L. F. (1989). Calcium buffer injections block fucoid egg development by facilitating calcium diffusion. *Proc. Natl. Acad. Sci. USA* **86**, 6607-6611.
Speksnijder, J. E., Sardet, C. and Jaffe, L. F. (1990). The activation wave of calcium in the ascidian egg and its role in ooplasmic segregation. *J. Cell Biol.* **110**, 1589-1598.
Sullivan, W., Daily, D. R., Fogarty, P., Yook, K. J. and Pimpinelli, S. (1993). Delays in anaphase initiation occur in individual nuclei of the syncytial Drosophila embryo. *Mol. Biol. Cell* **4**, 885-896.
Swann, K. and Whitaker, M. (1985). Stimulation of the Na/H exchanger of sea urchin eggs by phorbol ester. *Nature* **314**, 274-277.
Swope, R. E. and Kropf, D. L. (1993). Pronuclear positioning and migration during fertilization in Pelvetia. *Dev. Biol.* **157**, 269-276.
Taylor, A. R., Manison, N., Fernandez, C., Wood, J. and Brownlee, C. (1996). Spatial organization of calcium signaling involved in cell volume control in the fucus rhizoid. *Plant Cell* **8**, 2015-2031.
Tsien, R. Y. (1980). New calcium indicators and buffers with high selectivity against magnesium and protons: design, synthesis, and properties of prototype structures. *Biochemistry* **19**, 2396-2404.
Whitaker, M. (2006a). Calcium at fertilization and in early development. *Physiol. Rev.* **86**, 25-88.
Whitaker, M. (2006b). Calcium microdomains and cell cycle control. *Cell Calcium* **40**, 585-592.
Winkler, M. M., Steinhardt, R. A., Grainger, J. L. and Minning, L. (1980). Dual ionic controls for the activation of protein synthesis at fertilization. *Nature* **287**, 558-560.
Wokosin, D. L., Loughrey, C. M. and Smith, G. L. (2004). Characterization of a range of fura dyes with two-photon excitation. *Biophys. J.* **86**, 1726-1738.